Journal of Power Sources 192 (2009) 84–93

Contents lists available at ScienceDirect

Journal of Power Sources

journal homepage: www.elsevier.com/locate/jpowsour

Stirling based fuel cell hybrid systems: An alternative for molten carbonate fuel cells

D. Sánchez*, R. Chacartegui, M. Torres, T. Sánchez

Escuela Técnica Superior de Ingenieros de Sevilla, Camino de los descubrimientos s/n, 41092 Sevilla, Spain

ARTICLE INFO

Article history:
Received 30 September 2008
Received in revised form
25 November 2008
Accepted 13 December 2008
Available online 25 December 2008

Keywords:
Molten carbonate
Hybrid
Stirling

ABSTRACT

This paper presents a new design for high temperature fuel cell and bottoming thermal engine hybrid systems. Now, instead of the commonly used gas turbine engine, an externally fired – Stirling – piston engine is used, showing outstanding performance when compared to previous designs.

Firstly, a comparison between three thermal cycles potentially usable for recovering waste heat from the cell is presented, concluding the interest of the Stirling engine against other solutions used in the past.

Secondly, the interest shown in the previous section is confirmed when the complete hybrid system is analyzed. Advantages are not only related to pure thermal and electrochemical parameters like specific power or overall efficiency. Additionally, further benefits can be obtained from the atmospheric operation of the fuel cell and the possibility to disconnect the bottoming engine from the cell to operate the latter on stand alone mode. This analysis includes on design and off design operation.

1. Introduction

The main research and development areas in the electricity production industry are efficiency enhancement and pollutants reduction, especially carbon dioxide. Developing huge capacity facilities at one single location, in the range from 1 to 2 GW, is not a concern anymore as the scenario is shifting towards a more distributed scheme where electricity and heat are produced close to the final user. Additionally, conventional gas and steam combined cycle plants are currently producing around 1.5 GW, where needed, with off the shelf technology.

Advances in the suggested directions shall address the main concerns of today's society. First of all, some agents and observers of international politics along with scientists, mainly geologists, are claiming that a peak oil production rate is due to be reached in the following years, after which a reduction in oil production will have to be faced [1–3]. Consensus on the precise date does not exist but it is agreed that this situation shall take place in the first quarter of the present century. Despite the fact that coal seems to be abundant [4], high fuel to electricity conversions must be sought after if fuel consumption is to be reduced. This efficient production of electricity is profitable also in terms of emitted pollutants like carbon dioxide. If low temperature systems are developed, nitrogen oxides will be cut down as well.

In such a scenario, high temperature fuel cells have been regarded as very attractive power systems for small and even medium scale facilities of up to 1 MW rated capacity, showing a 50% stand alone efficiency. When coupled to gas turbine bottoming cycles, the efficiency of the resulting fuel cell – gas turbine hybrid system increases to 60% [5]. This concept has been applied to both solid oxide fuel cells and molten carbonate fuel cells with either open or closed bottoming cycles [6].

Hybrid systems have been researched for the past 15 years and, lately, they have approached the commercial phase [5,7,8]. Fuel Cell Energy (USA) has already completed field testing of its sub-megawatt proof of concept plant DFC/T, based on a 300-kW atmospheric MCFC coupled to an indirectly fired Capstone micro gas turbine. Ansaldo Fuel Cells (Italy) has also tested a hybrid MCFC/GT system successfully, based on two 250 kW 2TW pressurized cell modules coupled to an indirectly fired micro gas turbine. Finally, for the case of SOFCs, Siemens Westinghouse holds long experience with 220 kW and 300 kW demonstration units of directly fired gas turbines coupled to tubular cells.

Nevertheless, in spite of this previous experience with test plants, some problems regarding transient performance of hybrid systems seem to be still unresolved [9]. High temperature fuel cells require that air and fuel mass flows and temperatures be very precise in order to avoid undesirable situations like overheating or fuel/oxygen starvation. Thus, when they are coupled to bottoming gas turbines, and due to the very fast and sensitive transient performance of such engines, the control system turns out to be crucial in terms of operability and reliability. This concern is even more

* Corresponding author. Tel.: +34 954 48 64 88; fax: +34 954 48 72 43.
E-mail address: davidsanchez@esi.us.es (D. Sánchez).

0378-7753/$ – see front matter © 2008 Elsevier B.V. All rights reserved.
doi:10.1016/j.jpowsour.2008.12.061

Nomenclature

ΔH_f	enthalpy of reaction [kJ mol^{-1}]
A_{act}	cell active area [m^2]
C	compressor
CC	combustion chamber
CD	condenser
E	Nernst potential [V]
F	Faraday's constant
GT	gas turbine
HX	heat exchanger
j	current density [A m^{-2}]
MCFC	Molten Carbonate Fuel Cell
n	molar flow [mol s^{-1}]
OEM	Original Equipment Manufacturer
O&M	Operation and Maintenance
p	pressure [Pa]
Q	heat flow [kW]
R	gas constant
R_{cell}	cell resistance [Ω m^2]
SOFC	Solid Oxide Fuel Cell
ST	Stirling engine
T	temperature [K]
T	turbine
U_f	fuel utilization factor [%]
V	cell voltage [V]
X_i	molar fraction [–]

Subscripts

0	standard
amb	ambient
ano	anode
b	bottoming cycle
cat	cathode
ex	exhaust
ox	oxidation
shift	shift reaction

important when considering pressurized fuel cells fed by the gas turbine compressor directly [10].

In this work, an alternative bottoming cycle that may be able to solve some of the issues that are delaying the commercial availability of hybrid systems while, at the same time, maintaining high global efficiency is proposed. This proposal relies on an externally fired reciprocating Stirling engine for the bottoming cycle and an intermediate temperature fuel cell like ITSOFC or MCFC. MCFCs will be considered throughout this work due to their lower temperature and more mature technology. However, the same concept is applicable to SOFCs. As it will be shown, this layout allows for the fuel cell to be operated at atmospheric pressure and, additionally, the integration scheme permits to operate both systems as stand alone units, i.e. independently, what is an attractive feature for maintenance work and start up/shut down.

2. Heat recovery at intermediate temperature: Rankine, Brayton and Stirling

Thermal systems are frequently used for heat recovery in most heat-related industrial facilities as they allow for global fuel efficiency to be increased and even for environmental regulations to be complied with. These systems are generally defined by the following parameters:

1. Temperature at which the heat recovery process takes place.

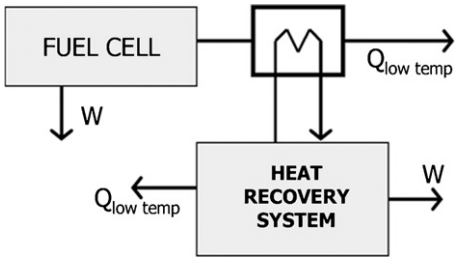

Fig. 1. Heat recovery concept applied to fuel cell systems.

2. Thermal power available to be recovered.

Waste heat is usually available in the form of a hot gas stream – for example, exhaust gases from a fuel cell – at a certain temperature, which establishes a limit for the bottoming cycle maximum temperature, following the general concept plotted in Fig. 1. According to this limit, a particular heat recovery cycle can be selected among the various possibilities available. In particular, three cycles are considered, as shown in Fig. 2:

1. Rankine cycle. Closed condensing cycle working on water/steam. Water is pumped to the turbine inlet through a heat recovery boiler where steam is generated. Steam is then expanded in the turbine and then condensed to water to start the cycle again. This system is usually regarded as the simple cycle and allows for a 25% cycle efficiency to be easily achieved. In order to increase this efficiency, water preheating with steam extracted from the turbine can be performed. Additionally, in order to further increase

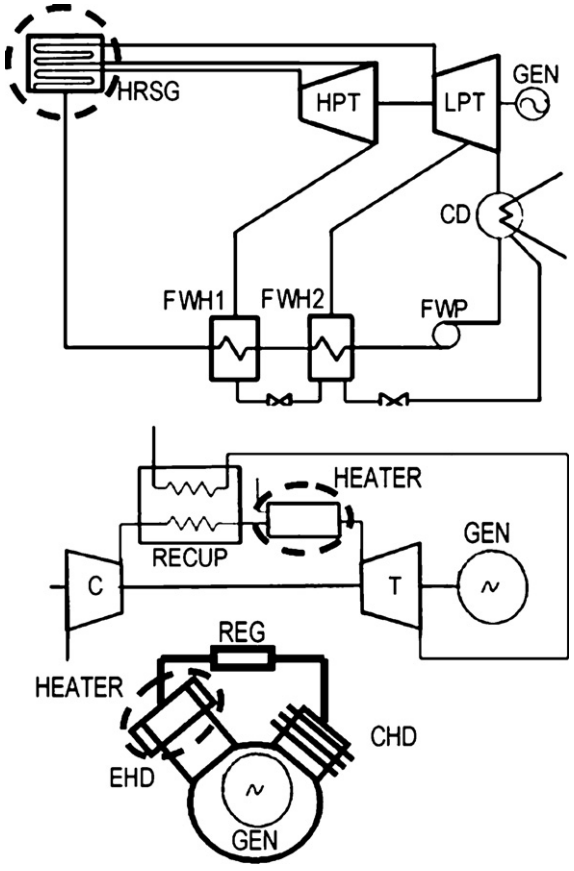

Fig. 2. Common heat recovery systems: preheat/reheat Rankine cycle (top), Recuperative Brayton cycle (center), Stirling engine (bottom).

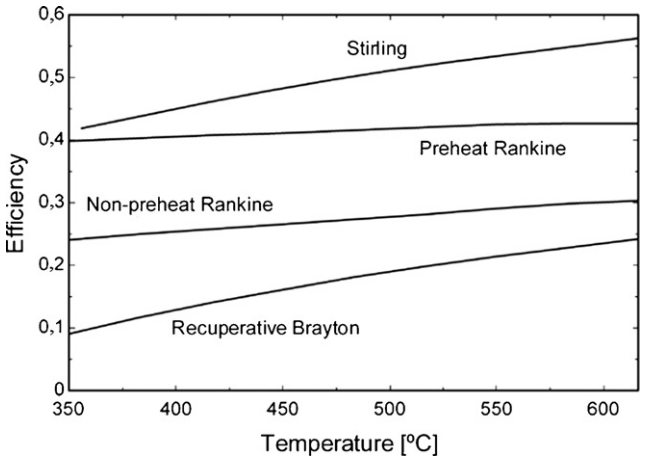

Fig. 3. Efficiency against reference temperature.

efficiency, steam can be extracted from the turbine at a partly expanded state, heated up again, and expanded to the condenser pressure. The latter innovation is known as reheating. If reheating and water preheating are introduced, a 45% cycle efficiency is possible.

2. Brayton cycle. Open non-condensing cycle working on air. Ambient air is compressed through a recovery heat exchanger and then expanded through a turbine with atmospheric exhaust. Small Brayton cycles make use of an exhaust gas recuperator to reduce the external thermal input. This heat exchanger is used to preheat the compressor delivery air with the turbine exhaust gases before it enters the heat addition device what, depending on the cycle, can increase the efficiency by around 10 percentage points. Some other cycle modifications have also been developed for this system but they are not used frequently, since its main attractive is simplicity and low cost against others.
3. Stirling cycle. Closed non-condensing cycle working on hydrogen or another gas with similar behaviour – helium, nitrogen. Unlike the previous systems, it is based on volumetric machinery. Ideally, a constant temperature compression is followed by a constant volume heat addition at the engine header. Hot gases are then expanded at constant temperature and, finally, cooled down at constant volume to start the cycle again. In order to reduce the external heat addition, a recuperator is usually installed. Cycle efficiencies in the range from 40 to 45% are easily achieved.

Fig. 2 shows the systems mentioned above. A reheat Rankine cycle is shown on top. Steam is generated at the HRSG (Heat Recovery Steam Generator) and expanded through the high pressure and low-pressure turbines, HPT and LPT, respectively. The exhaust steam is condensed at the condenser CD and pumped again to the steam generator through the feedwater preheaters FWH1 and FWH2, where its temperature is increased by a fraction of steam extracted from the turbine. For the Brayton cycle shown at the center of Fig. 2, a recuperator RECUP has been considered between the compressor C discharge and the external HEATER in order to increase the overall efficiency. This device recuperates energy from the turbine T exhaust gases. Finally, the bottom system in Fig. 2 depicts a simplified Stirling engine. The working gas is compressed at the compression header CHD, heated up at the regenerator REG and the external HEATER and then expanded at the expansion header EHD. In all three systems, mechanical power is converted into electricity at the generator GEN.

A comparison is shown in Fig. 3 where maximum cycle efficiency against temperature of available heat is shown for cycles in Fig. 2; this efficiency results from a thermodynamic analysis and does not include any irreversibility that is external to the system components (mechanical losses, pumping of cooling fluids, etc.). Starting from the worst performance, it can be assumed that Brayton cycles are not of any interest at this temperature level. Gas turbines are very sensitive to turbine inlet temperature since their operating principle relies in the variation of specific heat and volume with this parameter. When it is reduced, compression and expansion works become very similar and efficiency decreases dramatically. In other words, this loss in useful work cannot be compensated for by the reduction in heat addition due to the presence of a recuperator.

Rankine cycles seem to be interesting in Fig. 3 as they approach 40% when preheating is used. However, preheating is not feasible for these very small-scale power systems due to a much higher installation cost when several heat exchangers are present. This economic disadvantage discards the preheating Rankine cycle from the comparison shown in Fig. 3 and makes the performance of Stirling engines even more attractive. This latter alternative for heat recovery applications is far more interesting in terms of efficiency than any of the others and it suggests that a twofold improvement with respect to the conventionally used Brayton cycle is achievable.

These preliminary results in Fig. 3 have been obtained from an elementary thermodynamic analysis of the systems shown in Fig. 2. Rankine and Brayton cycles are simulated with lumped volume models developed with the general purpose thermodynamic package Engineering Equation Solver EES®. Input data of such models are collected in Table 1.

On the contrary, Stirling engines are not easily simulated since they are not formed by individual components performing single processes like Brayton or Rankine cycles. Instead, the reciprocating nature of its internal configuration establishes an interdependence of compression, expansion, heating and cooling of the working gas. To simulate this operation, Urieli's approach is used as shown in [11]. This model is implemented in EES® again with the input parameters shown in Table 1.

Now, having shown the potential of each heat recovery technology, the next step is to check the commercial availability of the

Table 1
Performance parameters for cycles considered in Fig. 2.

Parameter	Symbol	Value
Steam turbine		
High pressure turbine efficiency	η_{HPT}	0.85
Low pressure turbine efficiency	η_{LPT}	0.80
Feed water pump efficiency	η_{FWP}	0.80
Generator efficiency	η_{GEN}	0.98
Heat recovery steam generator	η_{HRSG}	0.70
Terminal temperature difference at FWH1 and FWH2	TDD_{FWH}	
Extraction pressures	–	20/3 bar
Feedwater heater 1 and 2 outlet temperature	–	212/133 °C
Live steam pressure/temperature	p_{LS}/T_{LS}	120 bar/540 °C
Condenser pressure	p_{CD}	0.05 bar
Gas turbine		
Compressor efficiency	η_C	0.85
Turbine efficiency	η_T	0.90
Generator efficiency	η_{GEN}	0.98
Recuperator effectiveness	R	0.80
Combustion chamber/heater efficiency	η_{HEATER}	0.90
Pressure ratio	PR	3:1
Stirling engine		
Engine efficiency	η_{ST}	0.38
Cooling water temperature (cold sink)	T_C	15 °C
Recuperator outlet temperature	T_{REC}	535 °C
Working gas		He

Table 2
Performance data of steam turbines (NA = not available; efficiency is turbine isentropic efficiency).

Manufacturer	Model	Mass flow [kg/s]	Power [kW]	Inlet [bar/°C]	Exhaust pressure [bar]	Efficiency [%]
Kaluga Turbine Works	ТП-320	1.21	235	13.7/194	1.2	~36
Dresser Rand	50/3600	0.28	37	42/400	2.75	~25
Jain Rotodyne	16H	NA	50–500	8–67/<510	0.2–10	NA
Shin Nippon	V-136	NA	<300	<46/<450	<8	NA

Table 3
Performance data of gas turbines (NA = not available; efficiency is engine efficiency).

Manufacturer	Model	Massflow [kg/s]	Power [kW]	Efficiency [%]
Capstone Inc.	C30	0.21	30	~26
Ingersoll Rand	MT250	2.13	250	~30
Calnetix	TA100	NA	100	~29
Turbec SpA	T100	0.80	100	~30

Table 5
Capital and O&M costs (1 € = 1.25 USD).

Technology	Installation cost		O&M cost	
	USD/kW	€/kW	cUSD/kWh	c€/kWh
Steam turbine	400–1500	320–1200	0.4	0.32
Gas turbine	900–1100	720–800	2.5	2
Stirling engine	2750–3000	2200–2800	15	12

necessary equipment (steam and gas turbines and Stirling engines) and determine its performance and cost. To do so, a power range of interest is set between 5 and 500 kW, depending on the system considered, which is suitable for molten carbonate fuel cells in the range from 10 to 750 kW, respectively.

Steam turbines in the range considered are usually single stage back pressure turbines (exhaust pressure above atmospheric pressure). Virtually all these turbines are found either at small CHP or cogeneration facilities, where the steam exhausting from the turbine is used as process steam, or driving feedwater pumps in conventional steam power plants, in which case they have vacuum exhaust pressure. The following companies, among others, supply this kind of equipment: Elliot Company (USA), Dresser Rand/Copus Steam Turbines (USA), Jain Rotodyne Private Ltd (India), Kaluga Turbine Works (Russia) or Shin Nippon Machinery Co. Ltd (Japan). Data regarding equipment from these manufacturers are shown in Table 2.

The availability of small scale gas turbines, usually referred to as micro gas turbines, is similar to steam turbines though, in this case, around 75% of the market share is hold by one single company, Capstone Turbine Corporation (USA), that manufactures 30 kW, 60 kW and 200 kW gas turbine engines. Nevertheless, the increasing interest in distributed energy systems is making more manufacturers offer this kind of equipment and, presently, several companies have similar products, like Table 3 shows: Ingersoll Rand Ltd (USA), Calnetix (USA) or Turbec SpA (Italy). Additionally, other companies and joint projects are developing similar systems: Wilson Turbopower (USA), Micro Turbine Technology B (The Netherlands) and the Belgian joint project powerMEMS, led by the Catholic University of Leuven (Belgium) are worth mentioning.

Finally, regarding Stirling engines, the first thing to remark is that the commercial availability of these engines is limited since this technology has not been widely used in any system or special application related to mechanical/electrical power production. Only in the field of concentrated solar power, these engines have always been considered as a very interesting alternative to steam cycles, although they have not ever been mass produced. Performance data of some modern and past engines are shown in Table 4.

Table 4 shows some interesting features. First of all, there are no Stirling engines with rated power higher than 50 kW. Second, the efficiency of currently available Stirling engines is around ten percentage points higher than commercial micro gas turbines in Table 3, this confirming the results from the thermodynamic analysis exposed in Fig. 3. This fact is very relevant since the steam turbines in Table 2 do not match the performance expected from Fig. 3 due to the effect of a reduced size on the internal efficiency of the turbine. Third and last, the previous results show that, despite the numerous research projects done in this field [12], Stirling engine manufacturers have had little commercial success. In fact, companies with a long experience in the design and manufacture of Stirling engines are not found presently.

Finally, to conclude with this review of existing technology, some data regarding estimated costs for the aforementioned equipment are given. For steam turbines, and since these machines do not work standalone but need complimentary equipment like condenser, pumps and boilers, estimators are usually applied to evaluate capital costs. This uncertainty is increased by the fact that most of these facilities are tailor made and their cost depends upon customer's requests strongly. Nevertheless, and according to the World Alliance for Decentralized Energy WADE, small non-reheat and non-preheat steam turbine cycles have installation costs in the range from 400 to 1500 USD/kW and O&M costs around 0.4 cUSD/kWh [13].

Installation costs of micro gas turbines can be estimated in 900–1000 USD/kW for electricity production equipment and 2500 USD/kW for combined heat and power utilities, this including the heat recovery part of the system, according to SCS Energy [14]. The same reference also quotes the O&M cost in 2.5 cUSD/kWh. This latter O&M cost is expected to be close to reality but, for the case of capital costs, care must be taken when applying these figures as long as considerable variation in cost per kilowatt might be found when ordering a high number of units to the same OEM.

Installation costs for Stirling engines are estimated in the range from 2750 to 3500 USD/kW for installation and 15 cUSD/kWh for O&M by the International Energy Agency [15]. All this information is summarized in Table 5 for the three technologies considered.

Table 4
Performance data of Stirling engines (NA = not available; *temporarily not commercially available).

Manufacturer	Model	Year developed	Power [kW]	Efficiency [%]	Maximum temperature [°C]	Commercially available
SES/Kockums (USA/Sweden)	4–95	1996	27	41	720	No
SES/Kockums (USA/Sweden)	4–275	1994	52.5	42	620	No
STM (USA)	4–120	1988	26.3	40–45	720	No
SOLO (Germany)	V-161	2001	9.2	30	650	No*
Stirling Danmark (Denmark)	SD-3	2006	35	18	NA	Yes
Stirling Biopower (USA)	PowerUnit	2008	40	30	NA	Yes

The following conclusions can be drawn from the review in this Section:

1. All the technologies considered to be potentially applicable to bottoming cycles in fuel cell hybrid systems are technologically and/or commercially immature. However, the Stirling engine is far behind both gas and steam turbines in all senses.
2. Although they seem to be economically interesting, steam turbines are not attractive due to their complexity. Among the others, the gas turbine is, for the time being, the most interesting choice in terms of costs and technological development.
3. However, as far as maximum efficiency is considered, the Stirling engine is the most interesting option with a clear advantage with respect to gas and steam turbines.

Conclusions 2 and 3 might seem contradictory but they are actually complementary. The immaturity of Stirling engines and the absence of mass production of these engines make their installation cost likely to be reduced significantly in the mid and long term. Such reduction will be due to technological development and economy of scale applied to the manufacturing process and, according to La Porta [16], it can be as high as 60% with respect to the values in Table 5. This fact highlights the potential of Stirling engines to substitute gas turbines in the bottoming cycles of fuel cell hybrid systems.

3. Molten carbonate fuel cell model

A molten carbonate fuel cell has been adopted for the hybrid system proposed in this work. In order to evaluate the performance of these systems, a simulation tool has been developed based on the work by Bosio et al. [17] and Iora and Campanari [18]. This is a three-dimensional model applicable to a generic cell layout but, since it has been calibrated against data from Ansaldo Fuel Cells, this work assumes this particular internal geometry. This assumption does not result in a lack of generality of any results obtained.

The model is based on an externally reformed cell whose ideal potential is evaluated through the following Nernst equation:

$$E = E_0 + \frac{RT}{2F}\ln\left(\frac{X_{H_2}\sqrt{X_{O_2}}X_{CO_2,cat}}{X_{H_2O}X_{CO_2,an}}\,\frac{P_{cat}^{3/2}}{P_{an}P_{amb}^{1/2}}\right) \quad (1)$$

where E_0 is the standard potential at ambient pressure, which varies almost linearly with temperature.

$$E_0 = 1.26485 - 2.4725\times10^{-4}\,T - 1.875\times10^{-8}\,T^2 \quad (2)$$

Different losses take place that make the real voltage of the cell V to be lower than the ideal Nernst potential:

$$V = E - j\cdot R_{cell} \quad (3)$$

where R_{cell} is the total equivalent resistance of the cell, expressed by Eq. (4), and j is the cell current density:

$$R_{cell} = \frac{A_{pol}e^{B/T}}{\prod_i p^{\beta_i}} + c_{iR} + D_{pol}\;e^{F/T} \quad (4)$$

The first term on the right-hand side of Eq. (4) stands for the contribution of both electrodes to the voltage loss and, from a practical point of view, only the effect of oxygen is relevant. Thus, only $i = O_2$ at the cathode is considered whereas the anodic side is neglected. The second term in Eq. (4) adds the effect of ohmic polarization at the internal cell contacts. Finally, the last term is related to the loss at the electrolyte and depends on the electrolyte content of the matrix – in this type of cells, a solid matrix is flooded by the molten salt – through a parameter D_{pol}. The values for all the parameters in Eq. (4) are shown in Table 6 and can be found in reference [18]. It is worth noting that parameters A, B, c, D and F are purely phenomenological and their values have been adjusted to fit experimental data of MCFCs.

Table 6
Parameters in Eq. (4) for reference geometry [18].

Parameter	Value
Apol [$\Omega\,m^2\,Pa^{0.67}$]	1.38×10^{-7}
B [K]	11400
ciR [$\Omega\,m^2$]	0.348×10^{-4}
Dpol [$\Omega\,m^2$]	4.8×10^{-8}
F [K]	6596
β_{O_2} [–]	0.67

An operating voltage V is selected and, as a result, a current density j is obtained when Eqs. (1)–(5) are solved simultaneously. The value of j is directly related with the amount of fuel consumed at the anode through Faraday's law and with the carbonate starvation in the electrolyte salt. Carbonate ions are responsible for the electronic charge transport between electrodes and, as shown in Eqs (6) and (7) for anode and cathode respectively, this causes that the concentration of carbon dioxide increases in the anode while decreasing at the cathode. Carbon dioxide must be therefore recirculated from anode exhaust to cathode inlet in order to keep the electrolyte composition as constant as possible [19]. Such mass/molar transfer must be accounted for when performing mass conservation calculations. In this work, gas leakages between electrodes, commonly known as cross-over, have been neglected in the assumption that pressure gradients between anode and cathode be sufficiently low [18,20].

$$\Delta n_{H_2} = -\frac{j\cdot A_{act}}{2F} = \Delta n_{CO_2,cat} = -\Delta n_{CO_2,ano} \quad (5)$$

$$H_2 + CO_3^{=} \rightarrow H_2O + CO_2 + 2e^- \quad (6)$$

$$(1/2)O_2 + CO_2 + 2e^- \rightarrow CO_3^{=} \quad (7)$$

Considering a certain amount of excess fuel, the total amount of hydrogen supplied to the cell is deduced from the fuel utilization factor U_f:

$$U_f = \frac{n_{H_2,consumed}}{n_{H_2,supplied}} \quad (8)$$

The model described in references [17,18] is based on a finite volume approach and applies mass and energy balances to individual grid elements in three coordinates. Such refinement is not needed for the present work and, instead, a lumped-volume approach is used, where global balances are calculated. Thus, considering the fuel cell to be a single control volume, the following energy balance can be used:

$$-n_{H_2,consumed}\Delta H_{ox} - n_{CO,shift}\Delta H_{shift} = W_{elec} + q_{ex}H_{ex} - q_{fuel}H_{fuel} - q_{air}H_{air} + Q_{loss} \quad (9)$$

Hydrogen oxidation and water gas shift are the only reactions occurring in the cell. For the former, the rate of reaction is calculated through Faraday's law, Eq. (5). For the latter, equilibrium at cell exhaust temperature is considered, according to the equilibrium constant expressed in [21]. The energy released when these reactions proceed is used to produce electrical work and to increase the sensible heat of the gases flowing through the cell, from fuel and air inlet to exhaust gases. Additionally, a certain amount of energy Q_{loss} is lost to the environment. This energy loss has been considered negligible throughout the simulations, though it can be given a certain value to adjust the model to experimental results. In the latter case, a quadratic dependence on current density, as shown in Eq. (10), gives good results.

$$Q_{loss} = a_0 + a_1\cdot j + a_2\cdot j^2 \quad (10)$$

Table 7
Input data for model calibration [18].

Parameter	Value	
Cell active area [m^2]	0.1	
Operating pressure [bar]	1.01	
Fuel flow [$Nm^3\ h^{-1}$]	0.259	
Oxidizer flow [$Nm^3\ h^{-1}$]	1.564	
Fuel/oxidizer inlet temperature [°C]	620	
Fuel composition [%vol]	H_2	21.2
	CO_2	18.7
	N_2	37.7
	H_2O	22.4
Oxidizer composition [%vol]	CO_2	9.8
	N_2	77.4
	O_2	12.8

Table 8
Model calibration [18].

j [$A\ m^{-2}$]	U_f (%)	V_{exp} [V]	V_{model} [V]	Error [%]
400	30.48	0.870	0.879	1.0
600	45.62	0.825	0.833	1.0
800	60.90	0.770	0.783	0.9
1000	76.15	0.730	0.717	−1.7
1200	91.22	0.675	0.667	−1.2
1250	94.92	0.660	0.655	−0.8

The model shown above has been calibrated against real experimental data from [18], pertaining to a stack manufactured by Ansaldo Fuel Cells, neglecting the heat lost to the environment, i.e. $a_i = 0$ in Eq. (10). Inputs to calibrate the model are shown in Table 7 while the results from this calibration are collected in Table 8 and drawn in Fig. 4, showing satisfactory agreement.

4. Molten carbonate fuel cell hybrid systems: comparison

Hybrid systems comprising Molten Carbonate Fuel Cells and bottoming heat engines are now compared. The concepts presented in Section 2 are slightly modified in order to be thermally integrated with the fuel cell model described in Section 3. The layouts of these systems are presented in Fig. 5.

A non-preheat Rankine cycle has been considered due to economical issues, as suggested previously. The excess fuel is burnt in a combustion chamber placed downstream of the boiler and the resulting combustion gases are used to preheat both the fuel and air streams feeding the fuel cell. Similarly, a combustion chamber is used in the MCFC-Brayton system to burn the excess fuel. These combustion gases flow through two preheaters, labelled HX2 and HX3 in Fig. 5. HX3 is used to heat up the working fluid of the bottoming cycle and HX2 is in charge of increasing the temperature of the partially preheated air and fuel at the fuel cell inlet. This first preheating took place at the recuperator HX1.

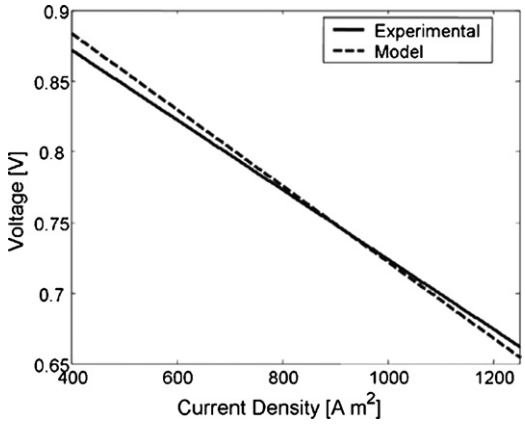

Fig. 4. Model calibration.

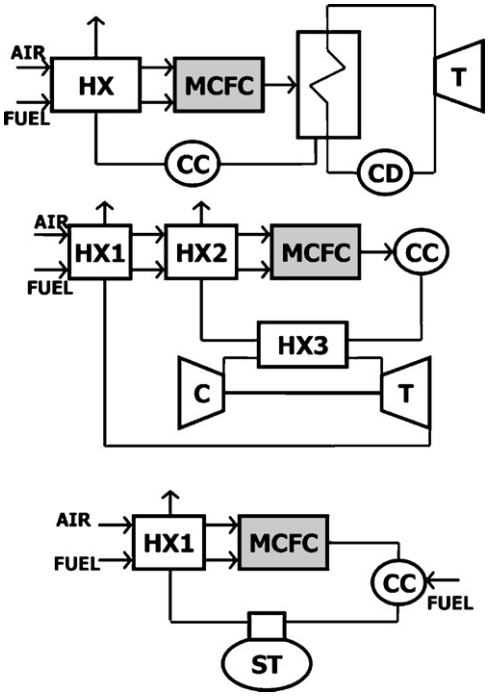

Fig. 5. Hybrid systems: bottoming Rankine (top), bottoming Brayton (center), bottoming Stirling (bottom).

A combustion chamber is also found at the MCFC-Stirling system but, this time, a small amount of additional fuel is burnt – with respect to the main fuel injection at the cell. The objective of burning additional fuel is to prevent the cell from a too high temperature gradient. If this fuel were not added, the outlet temperature of HX1 would be lower than recommended to guarantee the fuel cell integrity. It is worth noting that due to the very high cycle efficiency of the Stirling engines, similar to that of the fuel cell as shown in Fig. 3, adding fuel to be used in the bottoming cycle does not penalize the global efficiency of the system as it would do in a Brayton or Rankine cycle where, if this operation were adopted, a dramatic reduction in efficiency would be experienced. Nevertheless, since this additional fuel does not produce power at the fuel cell, it should be kept as low as possible. Eq. (11) shows the definition of system efficiency considered throughout the paper; W_{FC} and W_{bot} stand for fuel cell and bottoming cycle power and m_{fuel} and LHV are mass flow and low heating value of fuel.

$$\eta_{global} = \frac{W_{FC} + W_{bot}}{m_{fuel}LHV} = \frac{W_{tot}}{m_{fuel}LHV} \quad (11)$$

Results are shown in Table 9 for the systems presented in Fig. 5. The fuel cell is considered to operate at ambient pressure and 1000 $A\ m^{-2}$ current density in all cases, with 80% fuel utilization. Values are given for cell voltage, total specific power per unit cell active area, fraction of power produced by the bottoming cycle with

Table 9
Hybrid systems comparison.

	MCFC Rankine	MCFC Brayton	MCFC Stirling
j [$A\ m^{-2}$]	1000	1000	1000
V [V]	0.78	0.78	0.763
W [$kW\ m^{-2}$]	0.892	0.890	1.140
W_b/W_{tot}	0.123	0.121	0.278
η [%]	55.7	55.6	60.8

respect to total and system efficiency. The following aspects must be highlighted:

1. From the point of view of thermodynamics, there are not relevant differences between Rankine and Brayton based hybrid systems as they offer similar efficiencies. The bottoming cycle gives an additional 12% in both cases.
2. Due to the previous fact, Rankine cycles are not used in hybrid systems as they are more complex and costly than gas turbines, which are much more easily integrated with the fuel cell. Operation and maintenance costs are also higher when using high quality steam.
3. The Stirling engine offers an outstanding performance and supplies nearly half of the power of the fuel cell, one third overall. This excellent heat recover and conversion into useful work increases total efficiency by more than 5 percentage points for the case studied.

The statements above confirm that the Stirling engine is very interesting from the point of view of energy conversion. However, economical considerations must also be taken into account when assessing power systems and, according to Section 2, Stirling engines are still more expensive than steam and gas turbines by a factor of two approximately. Thus, even though Stirling engines are 25% more powerful for the same waste energy available, Table 9, the cost per kilowatt hour is still more expensive. However, the expected reduction in installation cost, as suggested in Section 2 previously, is likely to offset this disadvantage in the mid term.

5. MCFC-Stirling hybrid system: sensitivity analysis

This Section presents a sensitivity analysis of the hybrid system proposed in the previous Section with respect to off design and part load operation. These two operational modes are characterized mainly by modifications of fuel cell operating temperature and fuel cell current density respectively.

First of all, and in order to determine the performance of the bottoming cycle under such working conditions, performance maps are needed for the Stirling engine. These maps have been obtained with the aforementioned Urieli's model applied to a 45-kW engine, which is in the range of the most powerful engines commercially available today, according to Table 5. The efficiency of the engine at design condition, as obtained from the model, is 37% and the resulting performance maps are shown in Figs. 6 and 7. These figures present contour plots for generated power and engine exhaust temperature as functions of temperature and mass flow of inlet gas, respectively. It should be noted that both performance parameters depend mainly on inlet temperature, while the dependence on mass flow is quite weak. This is due to a variable speed control of part load operation being assumed for the engine.

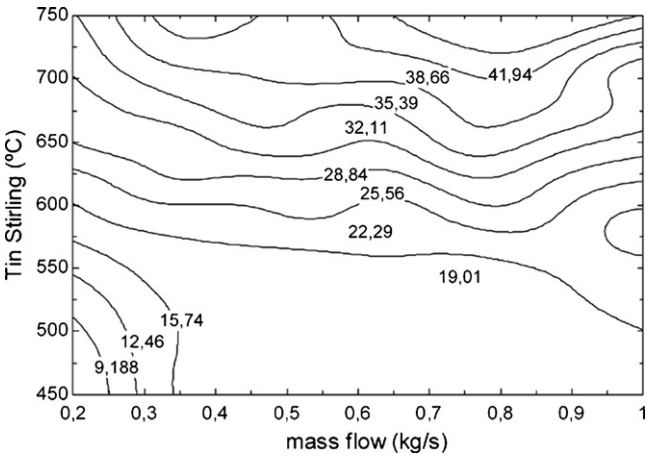

Fig. 6. Stirling engine performance map. Generated power [kW].

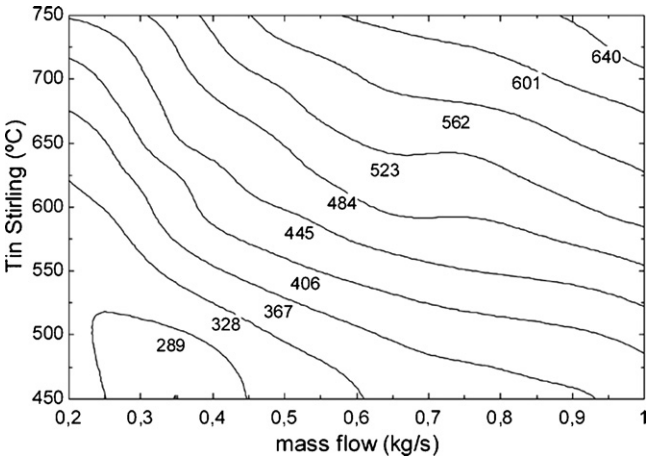

Fig. 7. Stirling engine performance map. Engine exhaust temperature [°C].

Modifications of the fuel cell current density are studied firstly. The heat balance of the hybrid system at design working conditions is shown in Fig. 8, where it is assumed that the Stirling engine performs according to Figs. 6 and 7. There is no additional fuel burnt in the second combustion chamber in Fig. 8, as indicated by the cross-symbol.

Figs. 9 and 10 show the effect of current density on efficiency and specific power, respectively, for different fuel cell operating temperatures. Different symbols and line types indicate these effects over the complete system and each of its components: fuel cell

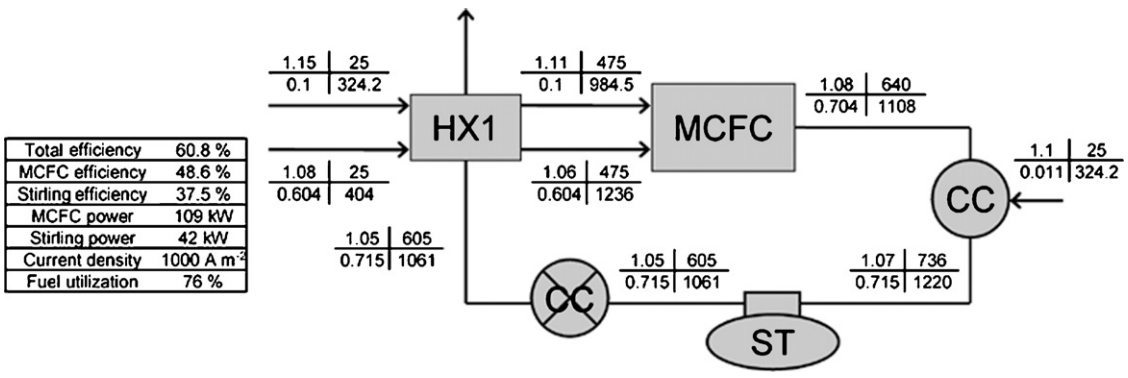

Fig. 8. Heat and mass balance for design point operation.

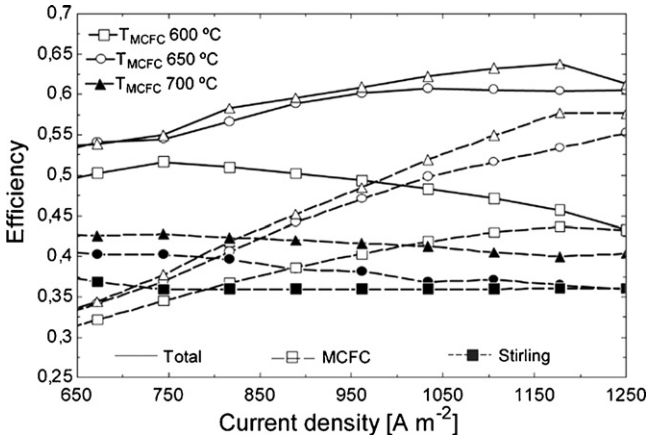

Fig. 9. Effect of current density on system efficiency.

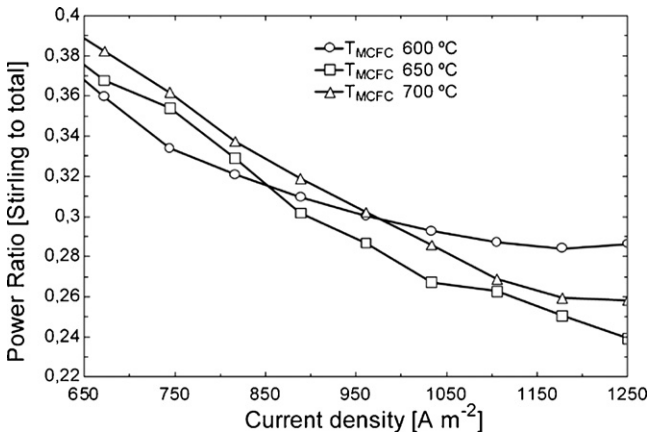

Fig. 11. Effect of current density on Stirling to total power ratio.

and Stirling engine. Some aspects of these curves must be discussed since they might seem contradictory. It is well known that fuel cell efficiency drops as current density increases but Fig. 9 shows the opposite behaviour. This is due to the operating line supplied by the manufacturer in reference [18] and shown in Table 8, where fuel utilization decreases with current density from 95% at 1250 A m^{-2} to 30% at 400 A m^{-2}. This penalty of reducing fuel utilization on efficiency prevails over the effect of current density and, as a consequence, the efficiency of the fuel cell increases at high current densities. On the contrary, in terms of specific power, Fig. 10 shows the usual parabolic shape which is characteristic of fuel cells.

With regard to the Stirling engine, both power and efficiency are quite independent from current density for a certain operating temperature of the fuel cell. There are two factors explaining this behaviour. In first place, as shown in Figs. 6 and 7, the efficiency of the engine depends on inlet gas temperature mainly and, to a much lesser extent, on the mass flow of inlet gases. Second, even though this latter dependence is weak, the inlet gas mass flow is quite constant for variable current density. Two are the opposite effects that explain this performance:

- when current density is reduced, the fuel mass flow required by the anode of the cell decreases and, therefore, so does the mass flow of exhaust gases.
- when current density is reduced, fuel utilization also decreases and, as a consequence, the excess fuel supplied to the anode of the cell is incremented. As a consequence, the mass flow of exhaust gases increases.

These contrary effects are well balanced and explain why the fuel cell exhaust mass flow is almost constant regardless the operating current density. Thus, as long as the temperature of the fuel cell does not change, efficiency and specific power of the Stirling engine are more or less invariable.

If system performance is now observed, global efficiency and total specific power decrease with current density at a more moderate rate than the efficiency of the fuel cell. Moreover, with regard to specific power, and since the performance of the bottoming system is somewhat constant, the fraction of total power that comes from the Stirling engine increases at part load. This is shown in Fig. 11 where it can be appreciated that the fraction of power produced by the Stirling engine increases by 45% approximately when current density drops from 1250 to 650 A m^{-2}, for any operating temperature. This is a very attractive feature of Stirling engines.

The analysis of cell temperature presented now is related to an abnormal operation of the hybrid system, inasmuch as the fuel cell must be operated at constant temperature in order to prevent thermal cycling and performance losses. This temperature control is usually done by modifying the excess air supplied to the cathode. Figs. 12 and 13 show the effect of cell temperature on specific power and efficiency where, again, different symbols and types of line have been used for system, fuel cell and Stirling engine data at three different current densities. For the fuel cell, efficiency and power decrease with temperature as it is expected from the increasing voltage losses, Eq. (4). For the Stirling engine, two opposite effects appear again:

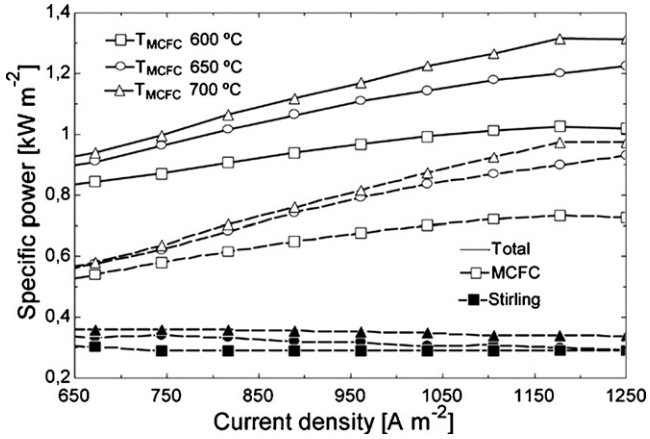

Fig. 10. Effect of current density on generated power.

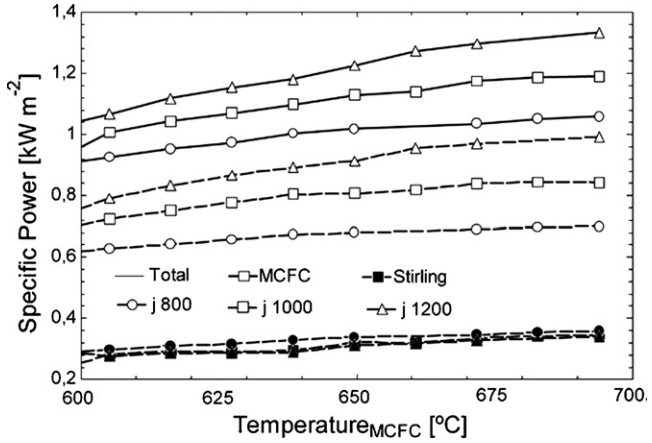

Fig. 12. Effect of cell operating temperature on generated power.

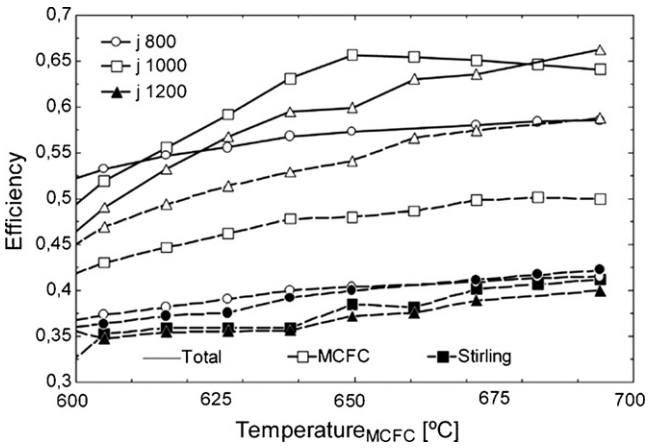

Fig. 13. Effect of cell operating temperature on efficiency.

- when cell temperature is reduced, engine efficiency drops as shown by the performance maps (Figs. 6 and 7).
- cell temperature is reduced by increasing the amount of excess air supplied to the cathode, this increasing the mass flow of inlet gas to the engine. As a consequence, engine power increases.

The power loss at the Stirling engine due to a reduction in inlet temperature is not compensated for by the increase in inlet mass flow and, consequently, engine power and efficiency decrease. It is worth noting that, as mentioned before, adding fuel at the combustion chamber located between cell and engine would increment the inlet temperature and offset this loss in engine efficiency. Yet, this is not advisable since the additional fuel does not produce power at the cell and, therefore, 40% of potential energy is not obtained.

The global effect over the hybrid system is that efficiency drops very rapidly with cell operating temperature below 650 °C and, to a lesser extent, the same happens to specific power.

From the analysis done in this Section for off design operation, it is concluded that the hybrid system proposed presents some very interesting features. Among others, it is interesting that total efficiencies above 45% and values for specific power around 1 kW m^{-2} are achievable at part load operation and usual operating temperatures, even though fuel utilization changes from rated values at design conditions. If this performance is compared with other analyses done by the authors in previous works [22], it is appreciated that the system proposed is more attractive that conventional gas turbine based systems.

Finally, some comments regarding part load control are needed. For the present analysis, a variable speed control has been assumed for the Stirling engine, considering this to be the most interesting control method from the point of view of manufacture and operation. Thus, while steam and gas turbines do suffer from low efficiency at part load operation, Stirling engines still perform well at reduced power settings. Steam turbines of this power range are usually operated by a control valve that reduces the amount of steam entering the turbine. Gas turbines operate at variable speed and pressure ratio while maintaining turbine inlet temperature as constant as possible in order to prevent efficiency from decreasing. Yet, gas turbines of this capacity have low part load efficiency even when integrated into hybrid systems, as shown by the authors elsewhere [22].

Stirling engines can be operated at part load in different ways: variable speed, variable hot gas temperature, variable maximum pressure or variable stroke are the most common. Among these, variable speed is very interesting since its efficiency is equal or even higher at part load than at design conditions, the rest of part load mechanisms being characterized by a reduced efficiency at part load [23]. However, adopting a variable speed implies that a power conditioning electronic system must be used to control the frequency of the power produced, as for the case of turbogenerators in micro gas turbines.

6. Conclusions

A concept for intermediate/high temperature fuel cell hybrid systems has been presented where a reciprocating engine is proposed for the bottoming cycle. This concept, though briefly presented previously, has not been studied in detail yet due to most efforts being concentrated on gas turbine based hybrid systems. Nevertheless, according to the simulations performed and shown in this paper, the Stirling engine has shown to be a potential competitor for conventional gas turbine hybrid systems, presenting improvements in terms of thermal performance and ease of operation with respect to the latter. The following issues have been observed:

1. When atmospheric fuel cells are considered, the Stirling engine based hybrid system is more efficient than Brayton or Rankine based systems, which are more or less equally efficient. In particular, the system presented in this work increases the efficiency of the system in 5 percentage points, breaking the 60% barrier.
2. As a matter of fact, hybrid systems formed by Stirling engine and atmospherically operated molten carbonate fuel cell are as efficient as some pressurized fuel cell and gas turbine systems developed in the past and currently undergoing tests programs [22]. This is remarkable since the very important effect of cell operating pressure on efficiency is not present in the system proposed.
3. It is expected that the system proposed does not present some of the reliability problems found by some manufacturers when operating fuel cells at high pressure, due to mechanical deterioration at sealing contacts/surfaces. Therefore, the Stirling and atmospheric fuel cell system is seen as competitive against the concept presently adopted by the majority of researchers/manufacturers in this field.
4. The hybrid system proposed seems to perform very well at off design conditions, this being one of the major improvements with respect to gas turbine hybrid systems currently available, especially those where the fuel cell is operated at high pressure.

The authors are currently developing more accurate models of performance that are capable of confirming the first results shown in this paper. Among others, detailed models of the Stirling engine working at transient conditions are under development with the objective of evaluating real operating conditions similar to test data available for conventional hybrid systems. For this purpose, an assessment of the most interesting part load operation strategy is necessary.

Eventually, when a detailed analysis is completed, a proof of concept system is to be developed. The availability of Stirling engines in the range from 10 to 100 kW sets the path to develop this project.

References

[1] R.W. Bentley, Energy Policy 30 (2002) 189–205.
[2] F. Leder, J.N. Shapiro, Energy Policy 36 (2008) 2840–2842.
[3] Q.Y. Meng, R.W. Bentley, Energy Policy 33 (2008) 1179–1184.
[4] N. Lior, Energy 33 (2008) 842–857.
[5] S. Campanari, P. Iora, P. Silva, E. Macchi, J. Fuel Cell Sci. Technol. 4 (2007) 308–316.
[6] D. Sánchez, R. Chacartegui, F. Jiménez, T. Sánchez, Proceedings of the ASME 2nd European Fuel Cell Technology and Applications Conference, Rome, 2007, pp. 61–62.
[7] A. Moreno, S. McPhail, R. Bove, International Status of Molten Carbonate Fuel Cell (MCFC) Technology, IEA/ENEA Report, January 2008.
[8] R.A. Roberts, J. Brouwer, J. Fuel Cell Sci. Technol. 3 (2006) 18–25.

[9] R.A. Roberts, J. Brouwer, E. Liese, R.S. Gemmen, J. Eng. Gas Turbines Power-Trans. ASME 128 (2006) 294–301.
[10] Siemens Power Generation, www.powergeneration.siemens.com (accessed July 2008).
[11] A.J. Organ, The Regenerator and the Stirling Engine, Mechanical Engineering Publications Limited, London, 1997.
[12] W.B. Stine, R.B. Diver, A compendium of Solar Dish/Stirling Technology, Sandia National Laboratories, DOE Contract n° 67-3678, 1994.
[13] World Alliance for Dencentralized Energy (WADE), www.localpower.org.
[14] J.L. Pierce, Intermountain CHP Application Center Workshop, Salt Lake City, August 2005.
[15] Renewables for Power Generation, Status and Prospects, International Energy Agency, Paris, 2003.
[16] F. La Porta, Technical and economical analysis of future perspectives of solar thermal power plants, PhD thesis, University of Stüttgart, 2006.
[17] B. Bosio, P. Costamagna, F. Parodi, Chem. Eng. Sci. 54 (1999) 2907–2916.
[18] P. Iora, S. Campanari, J. Fuel Cell Sci. Technol. 4 (2007) 501.
[19] K. Kordesch, G. Simader, Fuel Cells and Their Applications, 1st ed., Wiley-VCH, Weinheim, 1996.
[20] J.-H. Koh, B.S. Kang, H.C. Lim, J. Power Sources 91 (2001) 161–171.
[21] D. Sánchez, R. Chacartegui, A. Muñoz, T. Sánchez, J. Power Sources 160 (2006) 1074–1087.
[22] D. Sánchez, R. Chacartegui, T. Sánchez, J. Martínez, F. Rosa, Proc. Inst. Mech. Eng. Part A–J. Power Energy 222 (2008) 149–159.
[23] L.G. Thierme, D.J. Allen, Proceedings of the 21st Intersociety Energy Conversion Engineering Conference (IECEC), San Diego, 25–29 August, 1986.